Turbo Reconstruction of Structured Sparse Signals

Authors: Philip Schniter

Publication: Information Sciences and System (CISS), 2010

Speaker: Hyeong-ho Baek

Short summary**: This paper considers the reconstruction of structured-sparse signals from noisy linear observations. In particular, the support of the signal coefficients is parameterized by hidden binary pattern, and a structured probabilistic prior (e.g., Markov random chain/field/tree) is assumed on the pattern. Exact inference is discussed and an approximate inference scheme, based on loopy belief propagation (BP), is proposed. The proposed scheme iterates between exploitation of the observation-structure and exploitation of the pattern-structure, and is closely related to noncoherent turbo equalization, as used in digital communication receivers. An algorithm that exploits the observation structure is then detailed based on approximate message passing ideas.**

I. INTRODUCTION

The main objective is to estimate the sparse signal $\mathbf{x} \in \mathbb{C}^N$ from the noisy linear measurements $\mathbf{y} \in \mathbb{C}^M$,

$$\mathbf{y} = \mathbf{A}\mathbf{x} + \mathbf{w} \tag{1}$$

where $\mathbf{A} \in \mathbb{C}^{M \times N}$ is a known matrix and $\mathbf{w} \in \mathbb{C}^M$ is additive noise, often modeled as circular white Gaussian, i.e., $\mathbf{w} \sim CN(0, \sigma^2 \mathbf{I})$. By "sparse," we mean that the signal has only a few (say K, where $K << N$) non-zero coefficients.

In many cases of interest, the system of equations in (1) is underdetermined, i.e., $M << N$, so that, even in the noiseless case, there is no unique inverse. However, when $\mathbf{x}$ is known to be sparse, it is possible to accurately reconstruct $\mathbf{x}$ from $\mathbf{y}$ if the columns of A are sufficiently incoherent. For various sparse reconstruction algorithms, including convex- optimization-based,

greedy, and iterative thresholding algorithms, there exist elegant bounds on reconstruction error that hold when $\mathbf{A}$ satisfies a certain restricted isometry property (RIP). In many applications, however, the signal $\mathbf{x}$ has structure beyond simple sparsity. For example, the wavelet transform coefficients of natural scenes are not only approximately sparse, but also exhibit persistence across scales, which manifests as correlation within the sparsity pattern. Many other forms of structure in the sparsity pattern are also possible, and so we desire a powerful and flexible approach to modeling and exploiting such structure.

In this paper, we take a probabilistic approach to modeling sparsity structure, allowing the use of, e.g., Markov chain (MC), Markov random field (MRF), and Markov tree (MT) models [2]. Such models have been previously exploited for sparse reconstruction, but only to a limited extent. For example, [3] and [4] proposed Monte-Carlo-based [5] sparse reconstruction algorithms using MRF and MT models, respectively, and [6] and [7] proposed to iterate matching- pursuit with MAP pattern detection based on MRF and MT models, respectively. Monte-Carlo algorithms, while flexible, are typically regarded as computationally too expensive for many problems of interest. Matching-pursuit algorithms are typically much faster, but the schemes in [6], [7] are ad hoc. We attack the problem of reconstructing structured-sparse signals through the framework of belief propagation (BP) [8]. While BP has been successfully used to recover unstructured sparse signals (e.g., [9], [10]), we believe that its application to structured sparse signals is novel. As we shall see, the BP framework suggests an iterative approach, where sparsity pattern beliefs are exchanged between two blocks, one exploiting observation structure and the other exploiting pattern structure. In this regard, our scheme resembles turbo equalization from digital communications [11], where bit beliefs are exchanged between a soft equalizer and a soft decoder. Our two blocks are themselves naturally implemented using BP, and we detail a particularly efficient algorithm based on the approximate message passing (AMP) framework recently proposed by Donoho, Maleki, and Montanari [10].

II. Signal Model

Our structured-sparse signal model uses hidden binary indicators $\{s_n\}_{n=1}^N$, where $s_n \in \{0,1\}$. In particular, $s_n = 1$ indicates that the signal coefficient x_n is active while $s_n = 0$ indicates that

x_n is inactive. Assuming that the active signal coefficients are independently but non-identically distributed, we can write

$$p(x_n \mid s_n) = s_n q_n(x_n) + (1 - s_n)\delta(x_n) \tag{2},$$

Where $q_n(\cdot)$ denotes the pdf of x_n, when active, and $\delta(\cdot)$ denotes the Dirac delta. We refer to $\mathbf{s} = [s_1, s_2, \cdots, s_N]^T \in \{0,1\}^N$ as the sparsity pattern, and model structure in $\mathbf{s}$ through an assumed prior pmf $p(\mathbf{s})$.

III. Turbo Inference

Our primary goal is estimating the structured-sparse signal $\mathbf{x}$ given the observations $\mathbf{y} = \mathbf{y}_0$ in model (1). In particular, we are interested in computing minimum mean-squared error(MMSE) estimates of $\{x_n\}$.

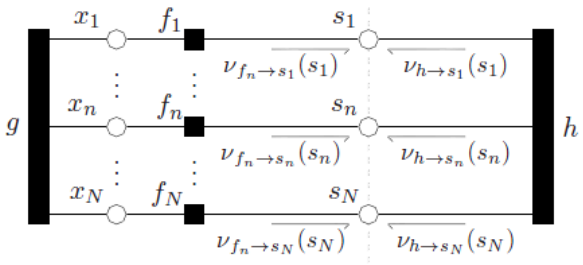

Figure 1 Factor graph of posterior $p(\mathbf{x}, \mathbf{s} \mid \mathbf{y} = \mathbf{y}_0)$. The boxes represent factor nodes and the circles represent variable nodes. Dashed line partitions the factor graph into two sub-graphs

A. Exact inference

The estimation task is facilitated by the following factorization of the posterior pdf shown by the factor graph in Fig. 1.

$$p(\mathbf{x}, \mathbf{s} \mid \mathbf{y} = \mathbf{y}_0) \propto p(\mathbf{y} = \mathbf{y}_0 \mid \mathbf{x}, \mathbf{s})\, p(\mathbf{x}, \mathbf{s}) = \underbrace{p(\mathbf{s})}_{\triangleq h(\mathbf{s})} \underbrace{p(\mathbf{y} = \mathbf{y}_0 \mid \mathbf{x})}_{\triangleq g(\mathbf{x})} \prod_{n=1}^{N} \underbrace{p(x_n \mid s_n)}_{\triangleq f_n(x_n, s_n)} \tag{3}$$

We use $\propto$ to denote equality after scaling to unit area.

The MMSE estimate of x_n is given by the mean of the marginal posterior $p(x_n \mid \mathbf{y} = \mathbf{y}_0)$, which can be written as

$$p(x_n \mid \mathbf{y}=\mathbf{y}_0) = \sum_{\mathbf{s}\in\{0,1\}^N} \int_{\mathbf{x}_{-n}} p(\mathbf{x},\mathbf{s} \mid \mathbf{y}=\mathbf{y}_0) = \sum_{\mathbf{s}\in\{0,1\}^N} \int_{\mathbf{x}_{-n}} \frac{p(\mathbf{x},\mathbf{s},\mathbf{y}=\mathbf{y}_0)}{p(\mathbf{y}=\mathbf{y}_0)} \tag{4}$$

$$\propto \sum_{\mathbf{s}\in\{0,1\}^N} \int_{\mathbf{x}_{-n}} p(\mathbf{x},\mathbf{s},\mathbf{y}=\mathbf{y}_0) = \sum_{\mathbf{s}\in\{0,1\}^N} \int_{\mathbf{x}_{-n}} p(\mathbf{s} \mid \mathbf{x},\mathbf{y}=\mathbf{y}_0)\, p(\mathbf{y}=\mathbf{y}_0 \mid \mathbf{x})\, p(\mathbf{x}) \tag{5}$$

$$= \sum_{\mathbf{s}\in\{0,1\}^N} \int_{\mathbf{x}_{-n}} p(\mathbf{s} \mid \mathbf{x})\, p(\mathbf{y}=\mathbf{y}_0 \mid \mathbf{x})\, p(\mathbf{x}) = \sum_{\mathbf{s}\in\{0,1\}^N} \int_{\mathbf{x}_{-n}} g(\mathbf{x})\, p(\mathbf{x} \mid \mathbf{s})\, p(\mathbf{s}) \tag{6}$$

$$= \sum_{s_n=0}^{1} f_n(x_n, s_n)\, p(s_n) \int_{\mathbf{x}_{-n}} g(\mathbf{x}) \prod_{q\neq n} \sum_{s_q=0}^{1} f_q(x_q, s_q) \sum_{\mathbf{s}_{-n,q}\in\{0,1\}^{N-2}} p(\mathbf{s}_{-n} \mid s_n) \tag{7}$$

Where $\mathbf{s}_{-n}$ denotes vector $\mathbf{s}$ with the n^{th} element omitted, and $\mathbf{s}_{-n,q}$ denotes $\mathbf{s}$ with both the n^{th} and q^{th} elements omitted. Writing $p(\mathbf{s}_{-n} \mid s_n) = p(\mathbf{s}_{-n,q} \mid s_q, s_n)\, p(s_q \mid s_n)$, the last summation in (7) reduces to $p(s_q \mid s_n)$, giving

$$p(x_n \mid \mathbf{y}=\mathbf{y}_0) \propto v_{f_n \to x_n}(x_n)\, v_{g \to x_n}(x_n) \tag{8}$$

$$v_{f_n \to x_n}(x_n) \triangleq \sum_{s_n=0}^{1} f_n(x_n, s_n)\, p(s_n) \tag{9}$$

$$v_{g \to x_n}(x_n) \triangleq \int_{\mathbf{x}_{-n}} g(\mathbf{x}) \prod_{q\neq n} \sum_{s_q=0}^{1} f_q(x_q, s_q)\, p(s_q \mid s_n) \tag{10}$$

B. Implementing the Message Passes

Whereas exact posterior calculation via (8)-(10) is computationally prohibitive for typical problem sizes, approximate calculation can be efficiently accomplished using message passing. Using the framework of BP, the functions $v_{f_n \to x_n}(\cdot)$ and $v_{g \to x_n}(\cdot)$ can be approximated.

$$v^{(t)}_{f_n \to x_n}(x_n) \propto \sum_{s_n=0}^{1} f_n(x_n, s_n)\, v^{(t)}_{s_n \to f_n}(s_n) \tag{11}$$

$$v^{(t)}_{g \to x_n}(x_n) \propto \int_{\mathbf{x}_{-n}} g(\mathbf{x}) \prod_{q\neq n} \underbrace{\sum_{s_q=0}^{1} f_q(x_q, s_q)\, v^{(t)}_{s_q \to f_q}(s_q)}_{v_{f_q \to x_q}(x_n) = v_{x_q \to g}(x_n)} \tag{12}$$

Which depend on the other messages

$$v^{(t)}_{s_n \to f_n}(s_n) = v^{(t)}_{h \to s_n}(s_n) \propto \sum_{\mathbf{s}_{-n}\in\{0,1\}^{N-1}} h(\mathbf{s}) \prod_{q\neq n} \underbrace{v^{(t-1)}_{s_q \to h}(s_q)}_{= v^{(t-1)}_{f_q \to s_q}(s_q)} \tag{13}$$

$$v^{(t)}_{f_n \to s_n}(s_n) \propto \int_{x_n} f_n(x_n, s_n) \underbrace{v^{(t)}_{x_n \to f_n}(x_n)}_{=v^{(t)}_{g \to f_n}(x_n)} \tag{14}$$

We use the superscript-(t) to denote iteration. These messages can then be combined for marginal inference:

$$p^{(t)}(x_n \mid \mathbf{y} = \mathbf{y}_0) \propto v^{(t)}_{f_n \to x_n}(x_n) v^{(t)}_{g \to x_n}(x_n) \tag{15}$$

$$p^{(t)}(s_n \mid \mathbf{y} = \mathbf{y}_0) \propto v^{(t)}_{f_n \to s_n}(s_n) v^{(t)}_{h \to s_n}(s_n) \tag{16}$$

Where $p^{(t)}$ denotes the iteration-t approximation to the pdf.

We now partition our factor graph into the two sub-graphs separated by the dashed line in Fig.1. The message $\left\{v^{(t)}_{f_n \to s_n}(\cdot)\right\}_{n=1}^{N}$ form the outputs of the left sub-graph and the inputs to the right one, while the messages $\left\{v^{(t)}_{h \to s_n}(\cdot)\right\}_{n=1}^{N}$ form the outputs of the right sub-graph and the inputs to the left one. From this, we can interpret the BP scheme as iterationg between two blocks, one which performs inference on the left sub-graph (which models structure in the observation) and the other which performs inference on the right sub-graph (which models structure in the sparsity pattern), with message-passing between blocks.

We will henceforth refer to inference on the left sub-graph of Fig.1 as "sparsity pattern equalization" (SPE) and inference on the right sub-graph as "sparsity pattern decoding" (SPD). We now formally decouple these subtasks and represent each of them using a separate factor graph, as in Fig. 2. For this, we define two additional t^{th} iteration constraint functions,

$$h^{(t)}_n(s_n) \triangleq v^{(t)}_{h \to s_n}(s_n) \tag{17}$$

$$d^{(t)}_n(s_n) \triangleq v^{(t-1)}_{f_n \to s_n}(s_n) \tag{18}$$

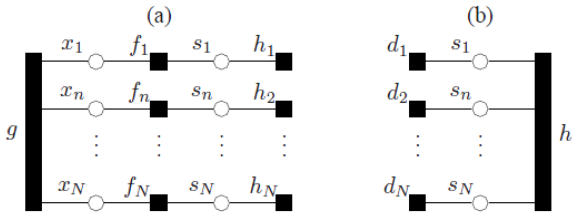

Figure 2 Decoupling of partitioned factor graph from Fig. 1 into
(a) sparsity pattern equalization and (b) sparsity pattern decoding.

IV. SPARSITY PATTERN EQUALIZATION

Below we outline a BP-based technique that follows the "approximate message passing" (AMP) framework recently proposed by Donoho, Maleki, and Montanari. Since we focus on a single iteration t, we suppress the superscript-(t) notation on messages in this section.

For BP-based SPE, we expand the g node in Fig. 2(a), yielding the loopy factor graph in Fig.3, with constraints

$$g_m(x) \triangleq CN(y_m; a_m^H \mathbf{x}, \sigma^2) \tag{19}$$

Where a_m^H denotes the m^{th} row of $\mathbf{A}$. Noting that SPE will require several iterations of message passing between nodes $\{g_m\}$ and $\{x_n\}$, we will henceforth use $v^i_{x_n \to g_m}$ and $v^i_{g_m \to x_n}$ to denote the SPE-iteration-i messages. In addition, we will assume Gaussian active-coefficients, i.e.,

$$q_n(x_n) = CN(x_n; 0, \sigma_n^2) \tag{20}$$

We use λ_n to abbreviate $h_n(1)$, the prior probability of $s_n = 1$ assumed by SPE. Thus, the coefficient is Bernoulli-Gaussian, with the form

$$v_{f_n \to x_n}(x_n) = \lambda_n CN(x_n; 0, \sigma_n^2) + (1-\lambda_n)\delta(x_n) \tag{21}$$

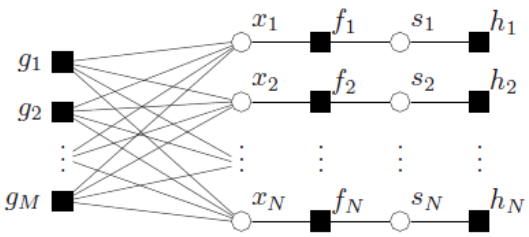

Figure 3 Factor graph for BP-based implementation of SPE

A. BP approximation via the large-system limit

Exact calculation of $v^i_{g_m \to x_n}(x_n)$ would involve the iteration of 2^{N-1} terms, which is cleary impractical. However, in the large system limit(i.e., $M, N \to \infty$ with M / N fixed), the central limit theorem motivates the treatment of $v^i_{g_m \to x_n}(x_n)$ as Gaussian. In this case, it is sufficient to parameterize the inputs to g_m via

$$\mu^i_{nm} \triangleq \int_{x_n} x_n v^i_{x_n \to g_m}(x_n) \tag{22}$$

$$v^i_{nm} \triangleq \int_{x_n} (x_n - \mu^i_{nm})^2 v^i_{x_n \to g_m}(x_n) \tag{23}$$

Which yields outputs from g_m that take the form

$$v^i_{g_m \to x_n}(x_n) \propto CN(A_{mn} x_n; z^i_{mn}, c^i_{mn}) \tag{24}$$

$$z^i_{mn} \triangleq y_m - \sum_{q \neq n} A_{mq} \mu^i_{qm} \tag{25}$$

$$c^i_{mn} \triangleq \sigma^2 + \sum_{q \neq n} |A_{mq}|^2 \mu^i_{qm} \tag{26}$$

From (22), (23), we see that μ^{i+1}_{nm} and v^{i+1}_{nm} are then determined by the mean and variance, respectively of the pdf

$$v^{i+1}_{x_n \to g_m}(x_n) \propto v_{f_n \to x_n}(x_n) \prod_{l \neq m} v^i_{g_l \to x_n}(x_n) \tag{27}$$

Using following equation

$$\prod_q CN(x; \mu_q, v_q) \propto CN\left(x; \frac{\sum_q \frac{\mu_q}{v_q}}{\sum_q \frac{1}{v_q}}, \frac{1}{\sum_q \frac{1}{v_q}} \right) \tag{28}$$

The product term in (27) reduces to

$$CN\left(x_n; \frac{\sum_{l\neq m} A_{\ln}^* z_{\ln}^i / c_{\ln}^i}{\sum_{l\neq m} |A_{\ln}|^2 / c_{\ln}^i}, \frac{1}{\sum_{l\neq m} |A_{\ln}|^2 / c_{\ln}^i} \right) \tag{29}$$

And so, under the large-system-limit approximations

$$c_{\ln}^i \approx c_n^i \triangleq \frac{1}{M} \sum_{m=1}^M c_{mn}^i \tag{30}$$

And $\sum_{l\neq m} |A_{\ln}|^2 \approx \sum_{l=1}^M |A_{\ln}| = 1$, (27) simplifies to

$$v_{x_n \to g_m}^{i+1}(x_n) \propto (\lambda_n CN(x_n; 0, \sigma_n^2) + (1-\lambda_n)\delta(x_n)) \times CN(x_n; \sum_{l\neq m} A_{\ln}^* z_{\ln}^i, c_n^i) \tag{31}$$

Applying (28) to (31), we find, after some algebra, that

$$\mu_{nm}^{i+1} = \alpha_n(c_n^i)\theta_{nm}^i / (1+\gamma_{nm}^i) \tag{32}$$

$$v_{nm}^{i+1} = \gamma_{nm}^i |\mu_{nm}^{i+1}|^2 + \mu_{nm}^{i+1} c_n^i / \theta_{nm}^i \tag{33}$$

$$\theta_{nm}^i \triangleq \sum_{l\neq m} A_{\ln}^* z_{\ln}^i \tag{34}$$

$$\gamma_{nm}^i \triangleq \beta_n(c_n^i) \exp(-\zeta_n(c_n^i) |\theta_{nm}^i|^2) \tag{35}$$

Where $\alpha_n(c) \triangleq \frac{\sigma_n^2}{c+\sigma_n^2}$, $\beta_n(c) \triangleq \frac{1-\lambda_n}{\lambda_n} \frac{c+\sigma_n^2}{c}$, $\zeta_n(c) \triangleq \frac{\sigma_n^2}{c(c+\sigma_n^2)}$.

The i^{th} SPE iteration yields the x_n-posterior approximation

$$p^i(x_n | \mathbf{y} = \mathbf{y}_0) \propto v_{f_n \to x_n}(x_n) \prod_{l=1}^M v_{g_{l\to x_n}}^{i-1}(x_n) \tag{36}$$

The mean and variance of (36) constitute the MMSE estimate of x_n and its MSE. Nothing that (35) differs from (27) only in the inclusion of the m^{th} product term.

B. Approximate message passing

The approximate BP algorithm outlined updates $O(NM)$ variables per iteration. When N and M are large, the resulting complexity may be undesirably high, motivating us to find a simpler scheme.

Recently, Donoho, Maleki proposed AMP algorithms that greatly simplify BP algorithms of the form outlined by tracking only $O(N)$ variables. Using AMP, we find that

$$\theta_n^i = \sum_{m=1}^{M} A_{mn}^* z_m^i + \mu_n^i \tag{37}$$

$$\mu_n^{i+1} = F_n(\theta_n^i; c^i) \tag{38}$$

$$v_n^{i+1} = G_n(\theta_n^i; c^i) \tag{39}$$

$$c^{i+1} = \sigma^2 + \frac{1}{M}\sum_{n=1}^{N} v_n^{i+1} \tag{40}$$

$$z_m^{i+1} = y_m - \sum_{n=1}^{N} A_{mn}\mu_n^{i+1} + \frac{z_m^i}{M}\sum_{n=1}^{N} F_n^{'}(\theta_n^i; c^i) \tag{41}$$

Above, $F_n(.;.)$, $G_n(.;.)$, and $F_n^{'}(.;.)$ are nonlinear functions that depend on the coefficient prior. We chose the Bernoulli-Gaussian prior. Thus, the nonlinear functions take the following form

$$F_n(\theta; c) = \frac{\alpha_n(c)}{1+\beta_n(c)e^{-\zeta_n(c)|\theta|^2}}\theta \tag{42}$$

$$G_n(\theta; c) = \beta_n(c)e^{-\zeta_n(c)|\theta|^2} \mid F_n(\theta; c)\mid^2 + \frac{c}{\theta}F_n(\theta; c) \tag{43}$$

$$F_n^{'}(\theta; c) = \frac{\alpha_n(c)}{1+\beta_n(c)e^{-\zeta_n(c)|\theta|^2}} \times \left[1 + \frac{\zeta_n(c)\mid\theta\mid^2}{1+(\beta_n(c)e^{-\zeta_n(c)|\theta|^2})^{-1}}\right] \tag{44}$$

V. Numerical Results

Numerical experiments were conducted for the observation model (1), where the elements of $\mathbf{A}$ were independently drawn from a $CN\left(0, \frac{1}{M}\right)$ distribution and where the signal coefficients were generated via $p(x_n \mid s_n) = s_n CN(x_n; 0,1) + (1-s_n)\delta(x_n)$ using Markov chain-generated binary sprsity pattern $\{s_n\}$. We set $\gamma \in (0,1]$ called the Markov independence parameter. Note

that, as γ increases, the pattern becomes less correlated, with $\gamma = 1$ corresponding to an i.i.d pattern.

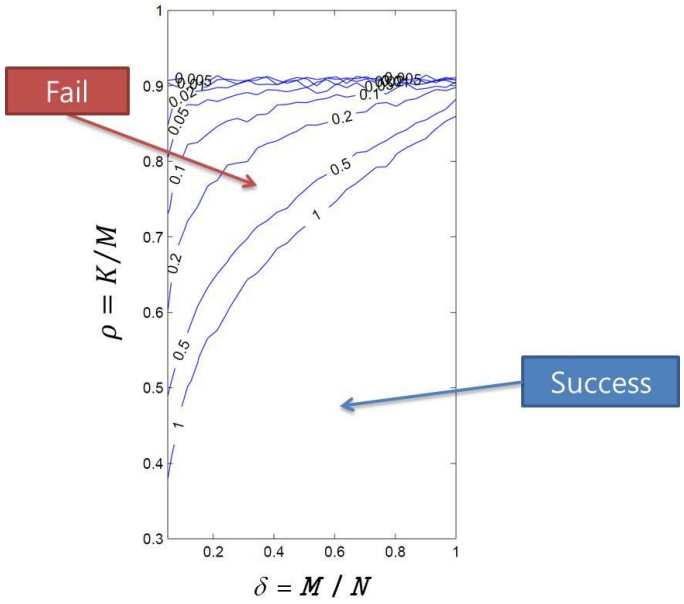

VI. DISCUSSION

After meeting, please write discussion in the meeting and update your presentation file.

Appendix

Reference

Compressive fluorescence microscopy for biological and hyperspectral imaging

Vincent Studer et al.

PNAS. (2012.12)

Presenter : Eunseok Jung

GIST, Dept. of Mechatronics , BiO-scopy Lab.

Gwangju Institute of Science and Technology

Background

- Fluorescence protein
  - Fluorescence microscopy use fluorescence protein.
  - Fluorescence protein can help to see molecule structure or phenomenon.

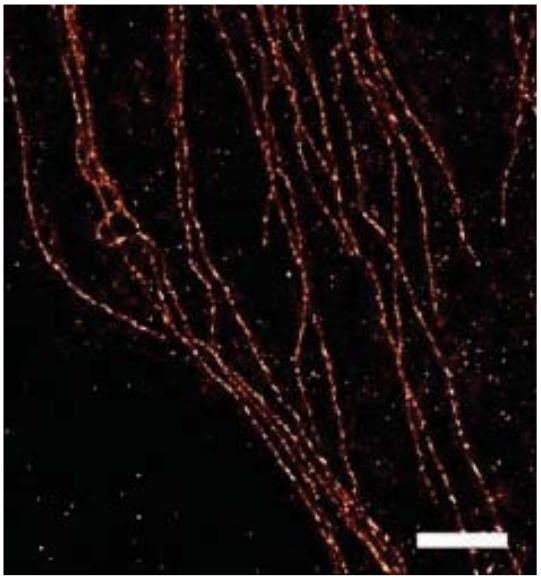

Cited form : http://huanglab.ucsf.edu, Wikipedia, http://www.microscopyu.com, http://smb.snu.ac.kr/tools_updating.htm

Introduction & Motivation

- CS algorithm make up fluorescence microscope major drawback

1. CS help to imaging in diffusing media.
2. CS can decrease experiment time.
3. If we use CS algorithm, it doesn't need expensive CCD camera.

From : Imaging Intracellular Fluorescent Proteins at Nanometer Resolution, E. Beitzig, science, 2006

System schematic

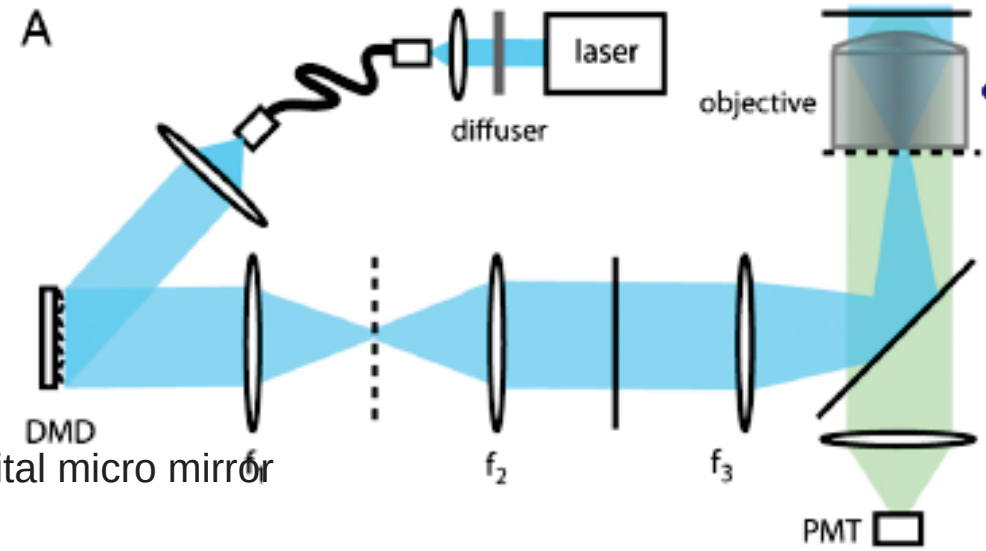

- Sample plane
- 60x objective lens
- Digital micro mirror
- Photo multiplier tube(Detector)

From : Imaging Intracellular Fluorescent Proteins at Nanometer Resolution, E. Beitzig, science, 2006

System schematic

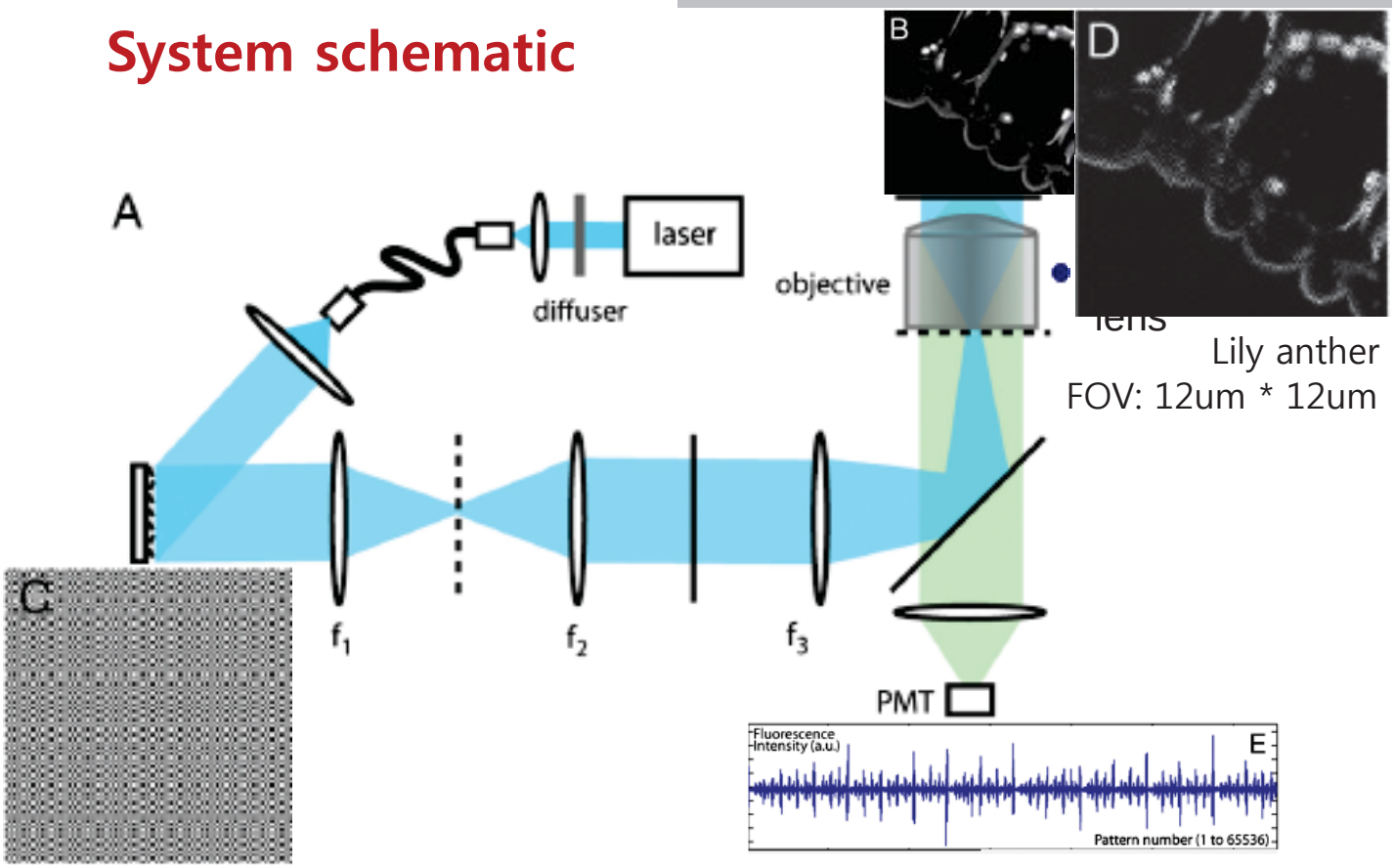

From : Imaging Intracellular Fluorescent Proteins at Nanometer Resolution, E. Beitzig, science, 2006

Reconstruction

$$\min_{\mathbf{x}\in\mathbb{R}^N} \|\mathbf{W}^T\mathbf{x}\|_{\ell_1} \text{ subject to } \|\mathbf{y}-\mathbf{\Phi x}\|_{\ell_2} \le \epsilon$$

- Recovering the signal x from acquired signal by solving the optimization problem.
- The acquired signal is noisy, it is better to relax the constraints into

$$\min_{\mathbf{x}\in\mathbb{R}^N} \|\mathbf{W}^T\mathbf{x}\|_{\ell_1} + \frac{\alpha}{2}\|\mathbf{y}-\mathbf{\Phi x}\|_{\ell_2}^2$$

- **W** will be either an orthonormal basis(e.g., Dirac basis) or an overcomplete signal representation(e.g., undecimated wavelet frame or curvelet frame).
- $\alpha(\epsilon)$ is chosen empirically depending on the noise level.

Reconstruction

- M=N/Under sampling-ratio.
- Under sampling ratio = 8, 16, 32, 64,...

  => M=8192, 4096, 2048,…
- It means, we can save the time to using this system.

N=256*256,
It was fixed by pixel

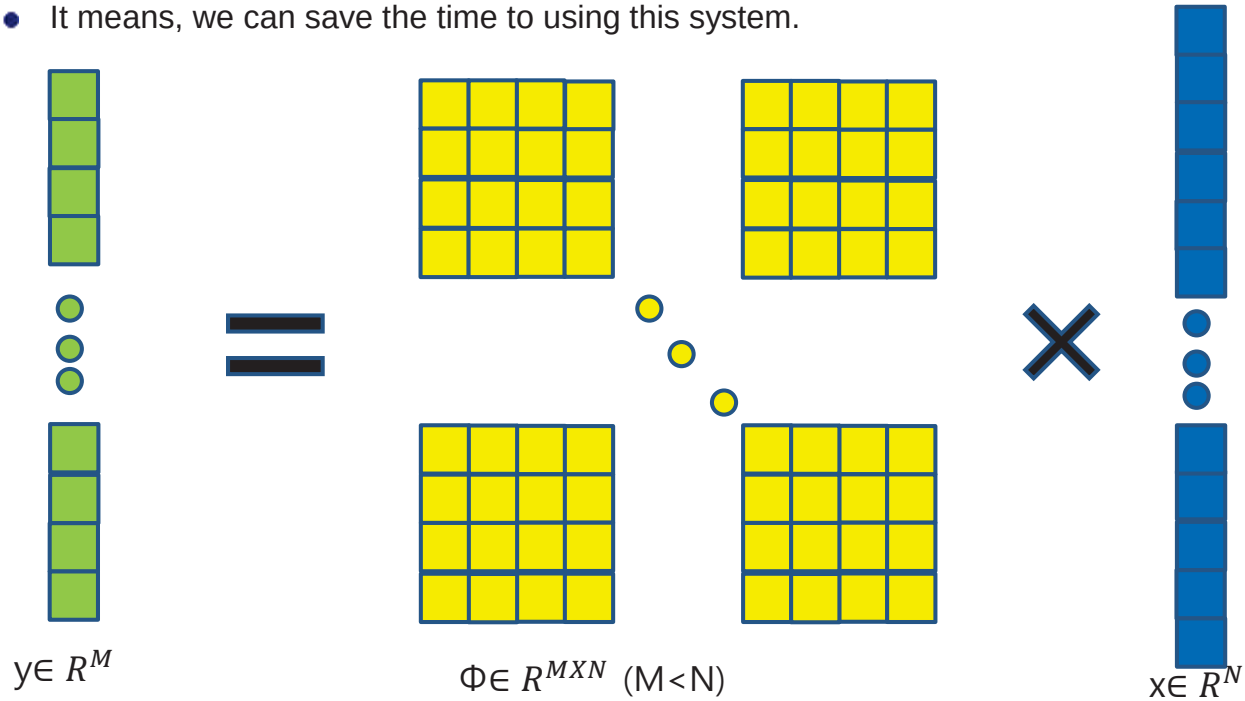

y∈ R^M Φ∈ R^{MXN} (M<N) x∈ R^N

Results

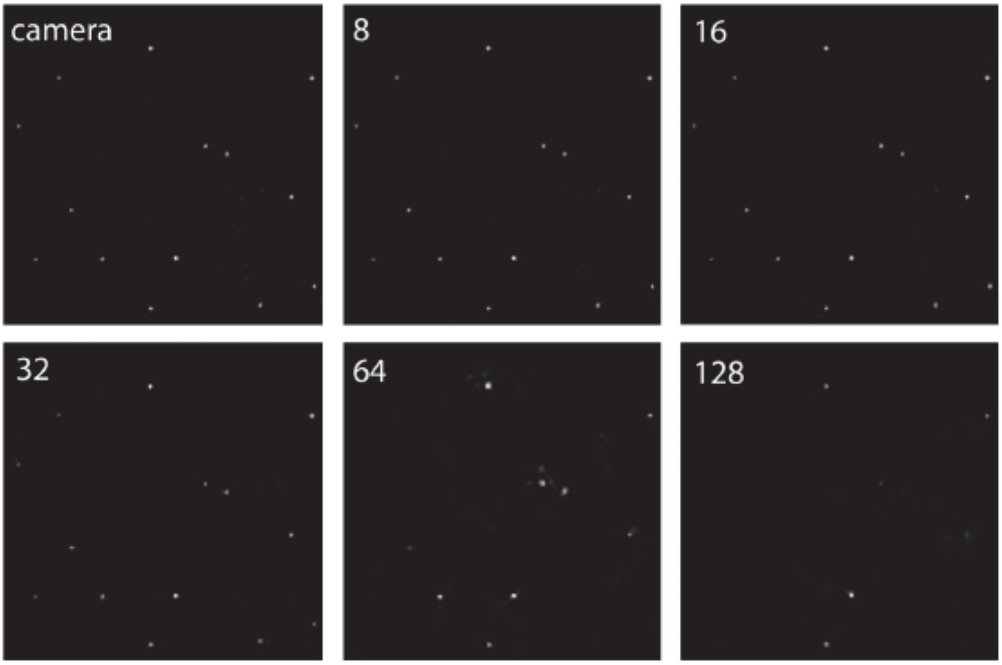

- Top left to bottom right: camera snapshot and reconstructed 256-by-256 bead images for values of the undersampling ratio equal to 8, 16, 32, 64, and 128.
- FOV: 6um * 6um

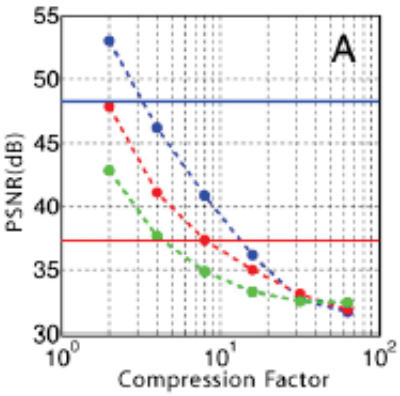

- Nominal illumination level(blue) and for the same level reduced by a factor 10(red) and a factor of 100(green). Solid lines correspond to the PSNR in raster scan for the same surfacic illumination(Blue: I, Red: I/10).

Simulation

		Random matrix	Hadamard matrix
		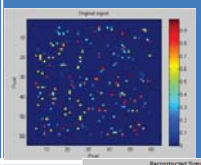	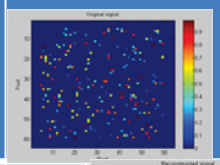
Rank : 1000	PSNR(dB)	78 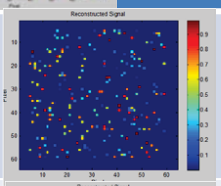	20 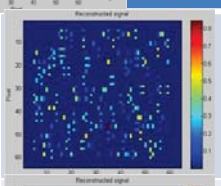
Rank : 2000	PSNR(dB)	87 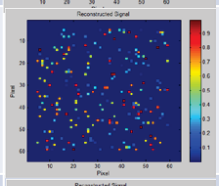	31 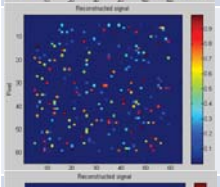
Rank : 3000	PSNR(dB)	88 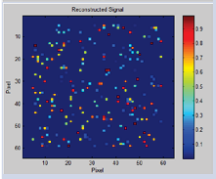	96 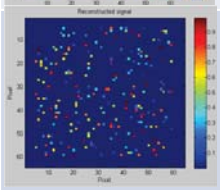
Rank : 4000	PSNR(dB)	90 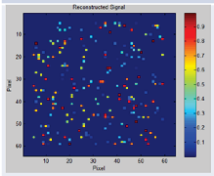	96 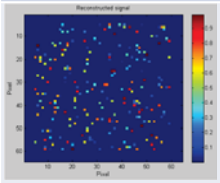

Discussion

- Conclusion

1. Reconstruct result is affected by measurement matrix.
   =>If we can make measurement matrix well, the reconstructed image will get high resolution image.

2. Fluorescence microscopy imaging is possible in diffusing media.

Thank you

Simplified Relay Selection and Power Allocation in Cooperative Cognitive Radio Systems

Authors: Liying Li et. al.

Publication: IEEE Trans. Wireless Comm., Jan. 2011

Speaker: Asif Raza

Short summary: In this paper authors propose solution of a combined problem; relay selection and power allocation to secondary users under the constraint of limited interference to primary users in cognitive radio (CR) system. Objective of the joint problem was to maximize system throughput. A high complexity optimal solution and a low complexity suboptimal solution are proposed. The presented solutions show over 50% improvement in system throughput.

I. INTRODUCTION

Cooperative technique for spectrum sensing and sharing in CR networks has been investigated in the literature. It can obtain spatial diversity and combat detrimental effects of wireless channels however it has some limitations associated. For example, while doing relay selection and resource allocation one must also consider spectrum efficiency and interference limitation as well. Authors in this paper consider these combined issues i.e. relay selection and power allocation with interference limitation.

II. SYSTEM DESCRIPTION

In order to have effective cooperation following decisions must be made prior to cooperation:

- When to cooperate
- To whom cooperate with
- What resources to share and how to share?

These decisions are basis of relay selection and power allocation problem.

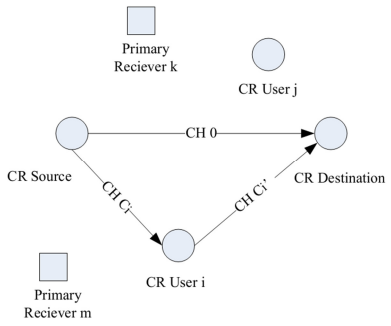

Figure 1: The structure of a cooperative CR network

A simple three-node relay system where each CR user can only help one CR transceiver pair is shown in the figure. The source node transmits data to the destination and the relay simultaneously using orthogonal channels, Channel (CH) 0 and CH C_i, respectively. The relay node forwards scaled version of the received signal from CH C_i to the destination node using CH C_i'.

Power modeling:

Existing relay selection schemes does not consider interference issue. In order to prevent primary users from interference the transmission powers on channels (CH 0), CH C_i and CH C_i' must satisfy:

$$\begin{aligned} P_{1,i}\left|h_{s,p,d}\right|^2 &\le I_1 \\ P_{2,i}\left|h_{s,p,i}\right|^2 &\le I_2 \qquad (1) \\ P_{3,i}\left|h_{i,p}\right|^2 &\le I_3 \end{aligned}$$

Where $h_{s,p,i}$ and $h_{s,p,d}$ are channel gain between CR source and primary users of CH C_i and (CH 0) respectively while $h_{i,p}$ is channel gain between CR source and primary user of channel CH C_i'. I_1, I_2 and I_3 are acceptable interference powers of primary users over channel CH 0, CH C_i and CH C_i' respectively. The overall transmission power of CR source and relay nodes are limited as:

$$P_{1,i} + P_{2,i} \le P_{total} \; and \; P_{3,i} \le P_3$$

The channels under consideration i.e. CH 0, CH C_i and CH C_i' are $\mathcal{N}(0, \sigma^2)$ with known channel gains at CR source and CR relay nodes. If ith CR user is relay node then signal and noise powers at destination from relay is:

$$P_{s,i} = \frac{P_{3,i}P_{2,i}\left|h_{s,i}\right|^2\left|h_{i,d}\right|^2}{P_{2,i}\left|h_{s,i}\right|^2+\sigma^2}$$

$$P_{n,i} = \left(\frac{P_{3,i}\left|h_{i,d}\right|^2}{P_{2,i}\left|h_{s,i}\right|^2+\sigma^2}+1\right)\sigma^2$$

$$SNR_i = \frac{P_{s,i}}{P_{n,i}}$$

Where $h_{s,i}$ and $h_{i,d}$ are channel gains between source and relay and relay and destination nodes respectively and SNR_i is SNR value at destination from ith relay channel.

Throughput Calculation:

The system throughput for ith relay is:

$$T_i\left(P_{1,i},P_{2,i},P_{3,i}\right)=\left(1-\alpha\right)\log 2\left(1+\frac{P_{1,i}\left|h_{s,d}\right|^2}{\sigma^2}\right)+\left(1-\alpha\right)\log 2\left(1+\frac{P_{3,i}\left|h_{i,d}\right|^2 P_{2,i}\left|h_{s,i}\right|^2}{\left(P_{3,i}\left|h_{i,d}\right|^2+P_{2,i}\left|h_{s,i}\right|^2+\sigma^2\right)\sigma^2}\right) \quad (2)$$

Where α is mis-detection probability of spectrum sensing.

This equation tells us that data will be lost if interference happens.

III. ALGORITHM DEVELOPMENT

Optimal and suboptimal algorithms are developed for power allocation and relay selection problem.

A. Optimal Approach

Optimization problem is formulated as:

$$\left(P_{1,i}^*,P_{2,i}^*,P_{3,i}^*\right)=\arg\max_{P_{1,i},P_{2,i},P_{3,i}} T_i\left(P_{1,i},P_{2,i},P_{3,i}\right) \quad (3a)$$

$$i=\arg\max_i T_i\left(P_{1,i}^*,P_{2,i}^*,P_{3,i}^*\right) \quad (3b)$$

subject to

$$P_{1,i}+P_{2,i}\le P_{total} \quad (3c)$$

$$P_{3,i}\le P_3 \quad (3d)$$

$$0\le P_{1,i}\left|h_{s,p,d}\right|^2\le I_1 \quad (3e)$$

$$0\le P_{2,i}\left|h_{s,p,i}\right|^2\le I_2 \quad (3f)$$

$$0\le P_{3,i}\left|h_{i,p}\right|^2\le I_3 \quad (3g)$$

Lagrange multiplier is then used to divide the problem into subproblems and then obtain solution for subproblems:

$$L\left(P_{1,i},P_{2,i},\lambda_1,\lambda_2,\lambda_3\right)=-\left(1-\alpha\right)\log_2\left(1+\frac{P_{1,i}\left|h_{s,d}\right|^2}{\sigma^2}\right)-\left(1-\alpha\right)\log_2\left(1+\frac{P_{3,i}\left|h_{i,d}\right|^2 P_{2,i}\left|h_{s,i}\right|^2}{\left(P_{3,i}\left|h_{i,d}\right|^2+P_{2,i}\left|h_{s,i}\right|^2+\sigma^2\right)\sigma^2}\right)$$
$$+\lambda_1\left(P_{1,i}+P_{2,i}-P_{total}\right)+\lambda_2\left(P_{1,i}\left|h_{s,p,d}\right|^2-I_1\right)+\lambda_3\left(P_{2,i}\left|h_{s,p,i}\right|^2-I_2\right) \quad (4)$$

According to Karush-Kuhn-Tucker conditions:

$$0\le P_{1,i},\ 0\le P_{2,i} \text{ and } \lambda_i\ge 0\ \ \forall i$$

$$\lambda_1\left(P_{1,i}+P_{2,i}-P_{total}\right)=0,$$
$$\lambda_2\left(P_{1,i}\left|h_{s,p,d}\right|^2-I_1\right)=0,$$
$$\lambda_3\left(P_{2,i}\left|h_{s,p,i}\right|^2-I_2\right)=0$$
$$and$$
$$\frac{\partial L}{\partial P_{1,i}}=0\,and\,\frac{\partial L}{\partial P_{2,i}}=0$$

Solving them by using dual-domain and sub-gradient method we get solution for Lagrangian dual variables as:

$$\lambda_1^{(n+1)}=\left[\lambda_1^n+\mu^n\left(P_{1,i}^n\left(\lambda_1^n,\lambda_2^n,\lambda_3^n\right)+P_{2,i}^n\left(\lambda_1^n,\lambda_2^n,\lambda_3^n\right)-P_{total}\right)\right]^+,$$
$$\lambda_2^{(n+1)}=\left[\lambda_2^n+\mu^n\left(P_{1,i}^n\left(\lambda_1^n,\lambda_2^n,\lambda_3^n\right)\left|h_{s,p,d}\right|^2-I_1\right)\right]^+,$$
$$\lambda_3^{(n+1)}=\left[\lambda_3^n+\mu^n\left(P_{2,i}^n\left(\lambda_1^n,\lambda_2^n,\lambda_3^n\right)\left|h_{s,p,i}\right|^2-I_2\right)\right]^+$$

Here 'μ^n' is sequence of scalar step-sizes. Once we get $\lambda_i,\forall i$ we can calculate $P_{1,i}$ and $P_{2,i}$ as follows;

$$P_{1,i}=\left[\frac{1-\alpha}{\left(\lambda_1+\lambda_2\right)\left|h_{s,p,d}\right|^2\ln 2}-\frac{\sigma^2}{\left|h_{s,d}\right|^2}\right]^+,$$
$$P_{2,i}=\left[\frac{\sqrt{P_{3,i}^2\left|h_{i,d}\right|^4+4P_{3,i}\left|h_{i,d}\right|^2\left|h_{s,i}\right|^2K}}{2\left|h_{s,i}\right|^2}-\frac{P_{3,i}\left|h_{i,d}\right|^2+2\sigma^2}{2\left|h_{s,i}\right|^2}\right]^+$$

Where $K=\frac{1-\alpha}{\left(\lambda_1+\lambda_3\right)\left|h_{s,p,i}\right|^2\ln 2}$ and $\left[\cdot\right]^+=\max\left(\cdot,0\right)$

By using these values we get optimal power allocation $P_{1,i}^*,P_{2,i}^*$. Note that $P_{3,i}^*=\min\left\{\frac{I_3}{\left|h_{i,p}\right|^2},P_3\right\}$.

Finally system throughput T_i^* when i[th] CR node acts as relay is then calculated from equation …

B. Sub-Optimal Approach

Joint relay selection and power allocation problem provides optimal throughput yet it is quite complex algorithm. A low complexity, sub-optimal version of the problem can be defined as follows:

Transmission power constraints of CR nodes are defined as:

$$P_{1,i} = \frac{I_1}{\left|h_{s,p,d}\right|^2}$$

$$P_{2,i} = \frac{I_2}{\left|h_{s,p,i}\right|^2}$$

In order to calculate system throughput by using equation 2 we need to choose relay as:

$$i = \arg\max_i \frac{P_{3,i}\left|h_{s,i}\right|^2\left|h_{i,d}\right|^2}{P_{3,i}\left|h_{i,d}\right|^2\left|h_{s,p,i}\right|^2 + I_2\left|h_{s,i}\right|^2 + \sigma^2\left|h_{s,p,i}\right|^2}$$

The optimal power limit and other constraints in (2) are taken as total power limit.

IV. Simulation Results

Parameters:

Interference limits:= $I_1 = I_2 = I_3 = 0.1mW$, Path loss exponent= 4, channel of unit bandwidth is used. Channel fading follows Rayleigh distribution with $\sigma = 6dB$

Results:

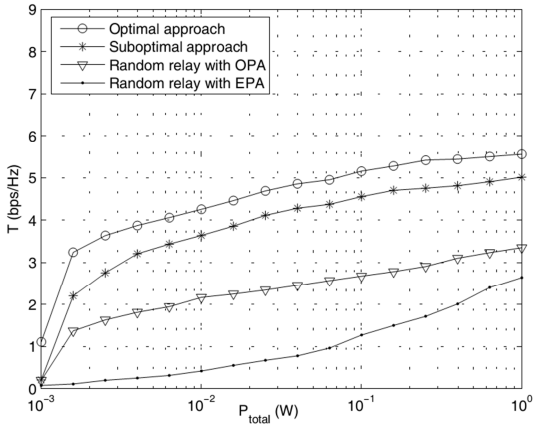

Fig. 2. System throughput versus transmission power limit of CR source

Transmission power limit of relay node is P_3 = 0.5W and no. of candidate relay nodes = 20 From figure we see proposed scheme achieves about 50% throughput achievement over optimal power allocation (OPA) and equal power allocation (EPA) schemes. Comparing sub-optimal scheme with optimal scheme we see only about 15% degradation in throughput is observed. Moreover in low P_{total} region the system throughput increase rapidly however for high P_{total} region the growth is restricted due to interference limits.

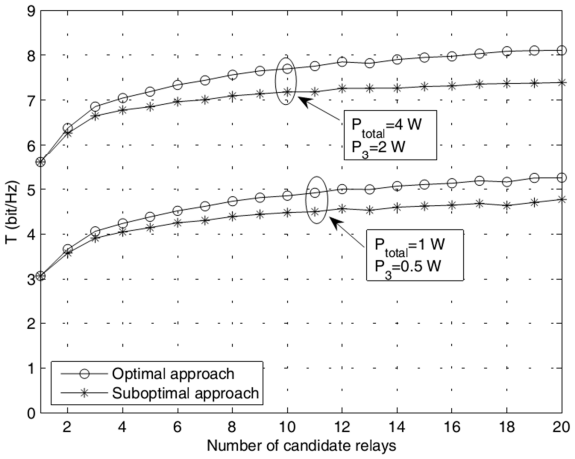

Fig. 3. System throughput versus number of candidate relays.

Figure 3 shows that gap between optimal and sub-optimal schemes is small well when the number of candidate users is small. This shows that sub-optimal approach performs well when number of relays are small.